

Effects of Stress on Martensite Transformation During Continuous Cooling and Mechanical Response of a Medium-Carbon High-Strength Steel



MAN LIU, GUANG XU, GUANGHUI CHEN, JUAN JIA, ZHENYE CHEN,
and ZILIU XIONG

The effects of stress on martensite transformation at different continuous cooling rates and the mechanical response of a medium-carbon high-strength steel were investigated by the metallographic method, dilatometry, and tensile tests. The results show that the microstructure consisted of martensite and retained austenite (RA) regardless of whether stress was applied. The martensite start temperature increased by stress due to additional mechanical driving force. The amount of martensite increased, while the amount of RA decreased at the same cooling rate by applying stress. In addition, the martensite laths were refined and variant selection of martensite orientation was observed by applying stress. Moreover, the tensile strength increased from about 1470 to 2170 MPa by applying stress because of more martensite and the fraction of low-angle grain boundaries. The strength improvement with the increase of cooling rate under stress was larger than that in the specimens without stress.

<https://doi.org/10.1007/s11661-019-05543-z>

© The Minerals, Metals & Materials Society and ASM International 2019

I. INTRODUCTION

MARTENSITIC transformation (MT), as characterized by its displacive shearlike nature, is one of the important means to strengthen steels.^[1,2] In order to better understand the kinetics of MT, it is necessary to analyze the martensite start temperature (M_s).^[3] The M_s is affected by many factors such as austenite grain size,^[4–7] cooling rate,^[8] and alloying element.^[9,10] For example, Yang and Bhadeshia^[4] established a suitable equation to describe the strongly dependent relationship between the M_s and austenite grain size. As austenite grain size decreases, both the M_s temperature and the amount of transformation product at room temperature decrease.^[7] Nikraves *et al.*^[8] reported that the M_s decreases at lower cooling rate if only martensite transformation occurs. Capdevila *et al.*^[10] revealed the influence of microalloying elements on the M_s and claimed that when the carbon concentration is lower (0.1 wt pct), the effect of microalloying elements on the M_s is small, while alloying elements have a greater

influence on the M_s if the carbon content is higher (0.8 wt pct). So far, many empirical relationships and models have been proposed to predict the M_s .^[11–14]

At the same time, the effects of deformation on MT were investigated by many researchers.^[15–18] It is reported that the ausforming can decrease the M_s , refine martensitic microstructure, and slightly increase hardness of a medium-carbon Si-Al-rich alloy steel.^[16] Other studies gave similar results. For example, Maalekian *et al.*^[17] reported that the M_s of a high-carbon low-alloyed steel decreases by deformation of austenite. A decrease in the M_s is also observed by hot deformation of Cu-P-Cr-Ni-Mo weathering steels.^[18] However, few studies focus on the effect of stress on MT during continuous cooling and the mechanical response of medium-carbon high-strength steels. It is certain that stress affects MT during continuous cooling.^[19,20] Hence, the purpose of the present study is to provide the theoretical reference for the control of martensite transformation during continuous cooling and mechanical properties of medium-carbon high-strength steels.

II. MATERIALS AND EXPERIMENTAL METHODS

The tested steel with a chemical composition of Fe-0.45C-2.03Si-2.81Mn (wt pct) was refined by a 50-kg vacuum furnace. High manganese was designed to stabilize austenite.^[21] The refined ingots were hot

MAN LIU, GUANG XU, GUANGHUI CHEN, and JUAN JIA are with The State Key Laboratory of Refractories and Metallurgy, Wuhan University of Science and Technology, Wuhan 430081, P.R. China. Contact email: xuguang@wust.edu.cn ZHENYE CHEN and ZILIU XIONG are with the HBIS Group Technology Research Institute, Hebei Iron and Steel Group Co., Ltd., Shijiazhuang 05000, P.R. China

Manuscript submitted July 27, 2019.

Article published online November 20, 2019

rolled on a 350-mm four-high mill to 12-mm plates. Cylindrical specimens of 6 mm in diameter and 86 mm in height for thermal simulation tests were prepared with hot-rolled plates. Thermal simulation experiments were conducted on a Gleeble 3500 simulator according to the procedures in Figure 1. Specimens were first austenized for 15 minutes at 1000 °C followed by cooling to ambient temperature at different cooling rates of 1, 5, and 10 °C/s, respectively, as shown in Figure 1(a). The specimens are termed N-1, N-5, and N-10, respectively. A compressive stress of 70 MPa was imposed on another group of specimens at different continuous cooling rates to investigate the effects of stress on MT and the mechanical response of the tested steel (Figure 1(b)). Specimens were austenized for 15 minutes at 1000 °C and then cooled to ambient temperature at different cooling rates under a compressive stress of 70 MPa during the entire cooling process. The specimens are termed S-1, S-5, and S-10, respectively. Stress loading was completed within 3 seconds. In addition, the real cooling rate was measured by thermocouples. The target cooling rate was achieved by adjusting the current based on the difference between the real and target cooling rates.

Specimens for microstructural observation were prepared by mechanical polishing and etching. Specimens were first ground with a series of SiC papers of decreasing granularity followed by polishing with diamond pastes. Then, the specimens were etched with 4 pct nital for a few seconds to reveal the microstructure. A Nova 400 Nano field emission-scanning electron microscope (SEM) equipped with electron backscatter diffraction (EBSD) was used to observe the microstructure and grain orientation at the acceleration voltage of 20 kV. To determine the volume fraction of retained austenite (RA), X-ray diffraction (XRD) experiments were carried out by a Bruker diffractometer using Co K_{α} radiation with a wavelength of 1.79 Å. The diffraction peaks, including (200)_α, (211)_α, (200)_γ, (220)_γ, and (311)_γ, were selected for quantitative analysis, and the following equation was used to calculate the amount of austenite^[22]:

$$V_i = \frac{1}{1 + G(I_{\alpha}/I_{\gamma})} \quad [1]$$

where V_i is the volume fraction of RA for each peak and I_{γ} and I_{α} represent the integrated intensities of austenite and ferrite peaks, respectively. The following G values for each peak are obtained from Reference 22: 2.46 for $I_{\alpha(200)}/I_{\gamma(200)}$, 1.32 for $I_{\alpha(200)}/I_{\gamma(220)}$, 1.78 for $I_{\alpha(200)}/I_{\gamma(311)}$, 1.21 for $I_{\alpha(211)}/I_{\gamma(200)}$, 0.65 for $I_{\alpha(211)}/I_{\gamma(220)}$, and 0.87 for $I_{\alpha(211)}/I_{\gamma(311)}$. In addition, tensile tests were carried out on a UTM-5305 electronic universal tensile tester at ambient temperature and the strain rate was $4 \times 10^{-3} \text{ s}^{-1}$. Three repeated tensile tests were performed for each test condition and the corresponding average values were obtained as the final results. The subsize specimens were prepared in the tensile tests due to the dimension limit of thermal simulation specimens. This might cause possible deviation in tensile properties. However, the tensile properties of different specimens were comparable based on the same sample size.

III. RESULTS AND DISCUSSION

A. Microstructure

Figure 2 gives the typical SEM microstructures of specimens under different stress states and cooling rates. According to the classification method, to identify the microstructure proposed in Reference 23, it can be observed that the microstructures of all specimens consist of martensite and RA. Thus, the decomposition of austenite into ferrite and bainite was avoided at cooling speeds of 1, 5, and 10 °C/s. The early transformed martensite was autotempered during the cooling process, which is confirmed from the existence of concave martensite blocks, as pointed out by the arrows in the dashed rectangle and enlarged image in Figure 2(c). In addition, the martensite laths became finer with the increase of cooling rates regardless of whether stress was applied. This may be attributed to the fact that a higher cooling rate cannot provide

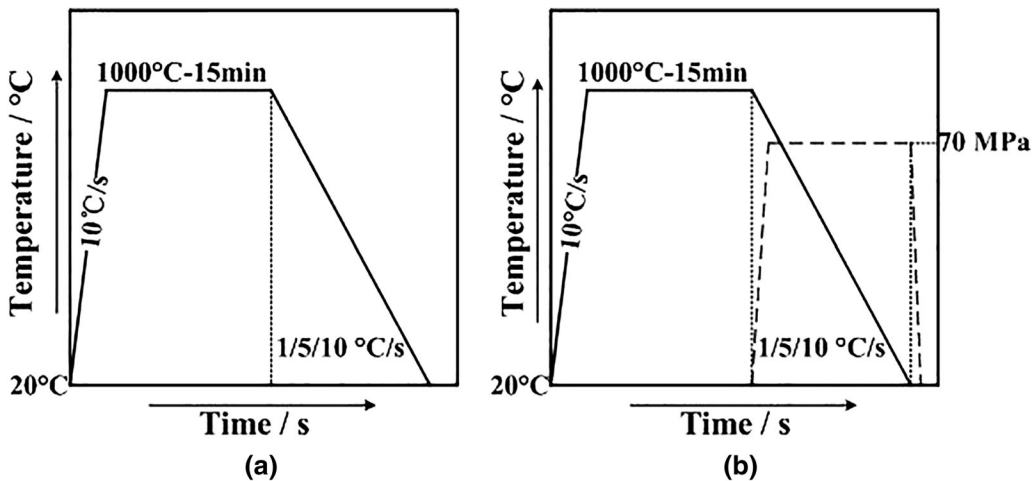


Fig. 1—Schematic of experimental procedures: (a) continuous cooling without stress and (b) continuous cooling with compressive stress.

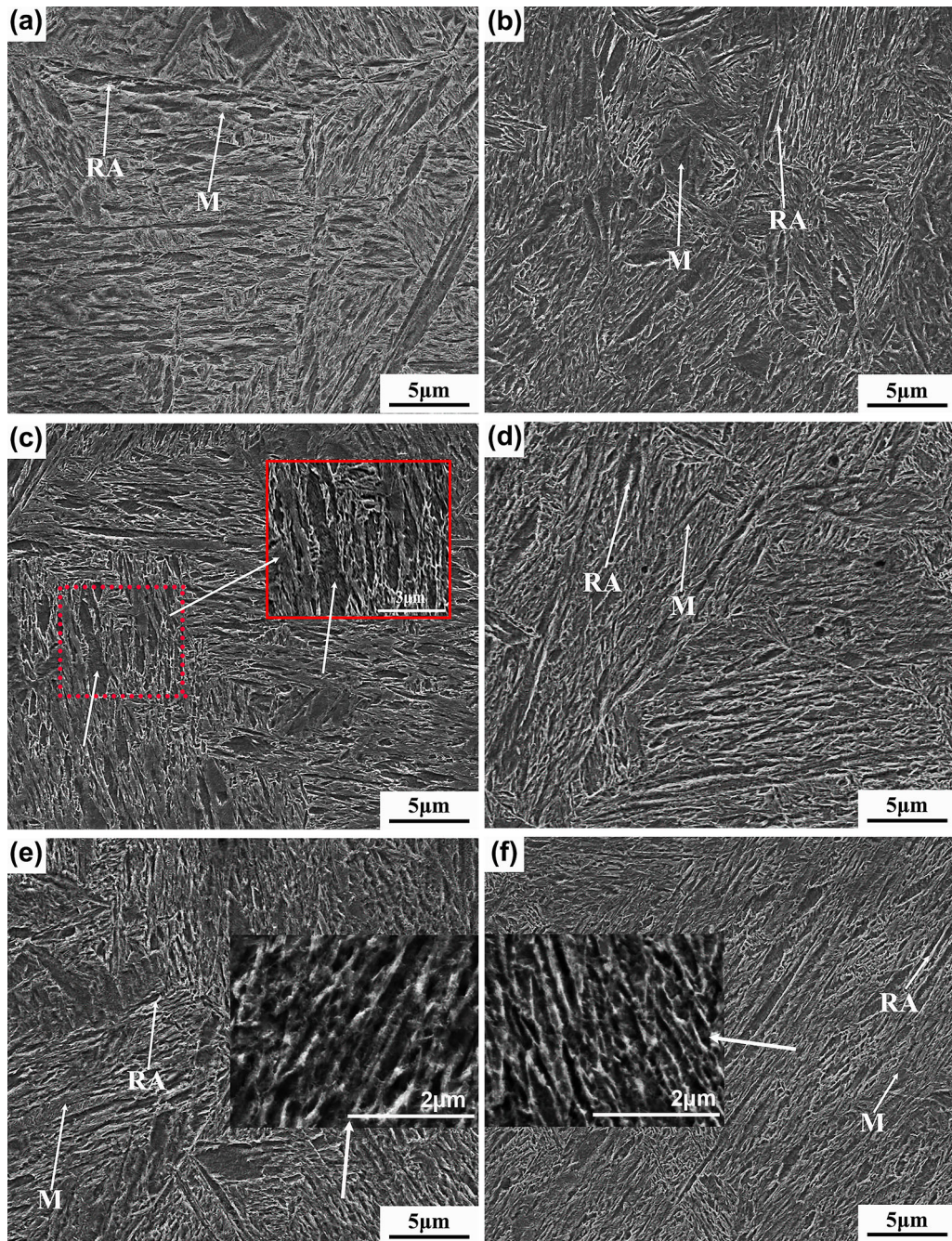


Fig. 2—SEM microstructures of different specimens: (a) N-1, (b) S-1, (c) N-5, (d) S-5, (e) N-10, and (f) S-10.

sufficient time for the growth of martensite; thus, the martensite laths are finer compared to those in the specimen at smaller cooling rates. Moreover, compared to the specimens without stress, the martensite laths of specimens with stress were further refined, which is clearly observed in enlarged images by arrows in Figures 2(e) and (f). This is because a plastic deformation was induced by stress due to the lower yield strength of austenite at high temperature, resulting in the refinement of original austenite grains. In the subsequent cooling process, the growth of martensite

was restrained by the packet and the block martensite boundaries, the grain boundaries, and the dislocations in grains, resulting in the formation of finer martensite laths. Moreover, it is expected that the dynamic recrystallization of austenite and the acceleration of MT occurred due to the plastic deformation of austenite. Thus, the microstructure was refined due to the deformation of austenite at high temperature. On the other hand, more fine martensite forms due to the additional mechanical driving force and more nucleation sites induced by stress.

B. Dilation

Figure 3 illustrates the dilation curves of specimens under different stress states and cooling rates. The dilation curves are obtained by measuring the change of specimen diameters. The dilation curves are the results of volume shrinkage caused by cooling and dilation caused by transformation. The amount of dilation is a function of temperature. A sharp increase in dilation from point A to B in Figure 4(b) is caused by a deformation due to the increase of compressive stress from 0 to 70 MPa. Also, the strains in specimens S-1,

S-5, and S-10 caused by stress were calculated to be 4.42, 3.95, and 2.32 pct, respectively. According to the microstructural results (Figure 2), only MT occurred during continuous cooling. The tangent method was adopted to determine the M_s . Thus, the M_s values of different specimens were determined and are shown in Figure 3 and Table I. This indicates that the M_s of specimens decreases with the increase of cooling rates regardless of whether stress is applied. More importantly, at the same cooling rate, applying stress during continuous cooling results in the increase of the M_s .

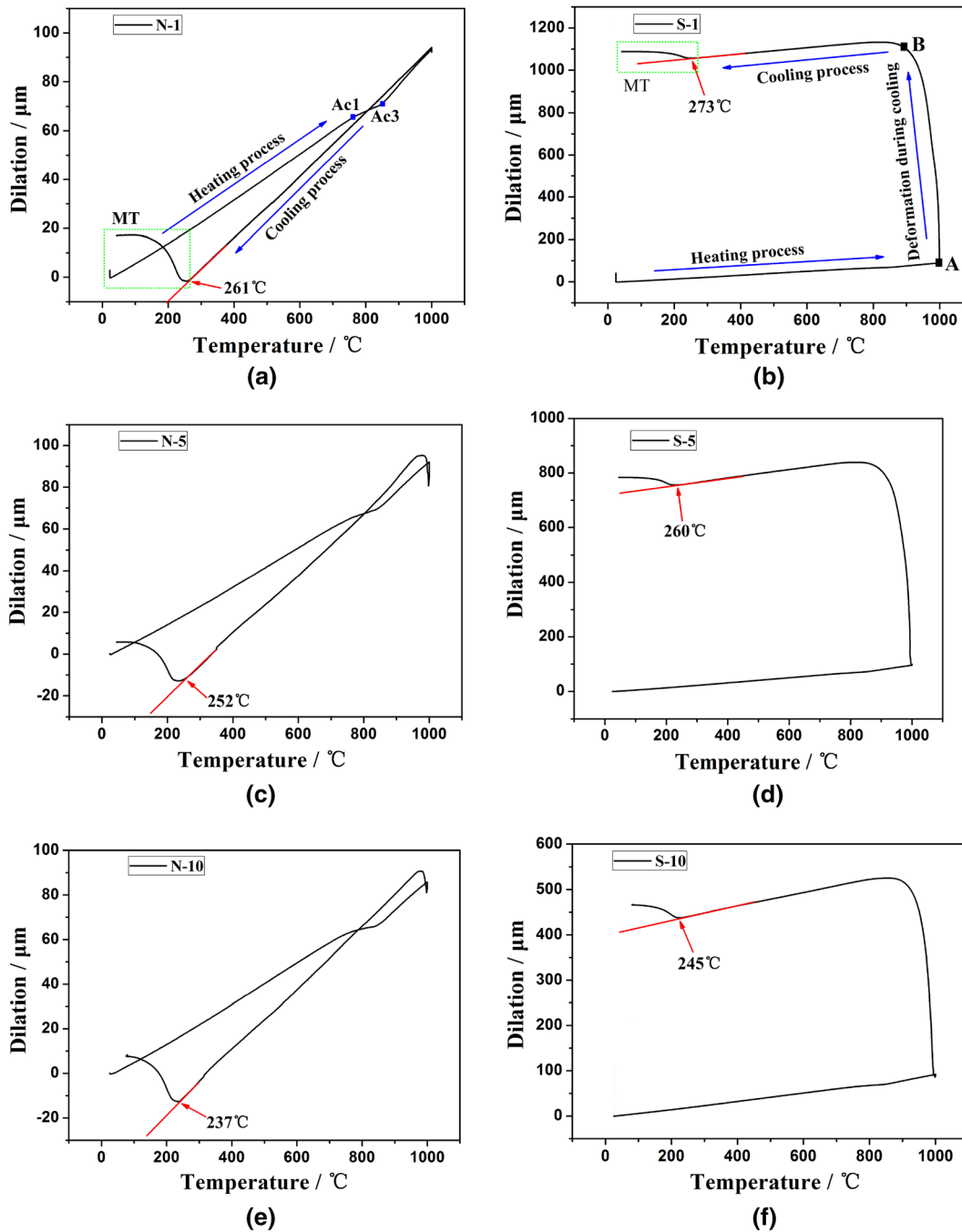


Fig. 3—Dilation curves of different specimens along the diameter direction: (a) N-1, (b) S-1, (c) N-5, (d) S-5, (e) N-10, and (f) S-10.

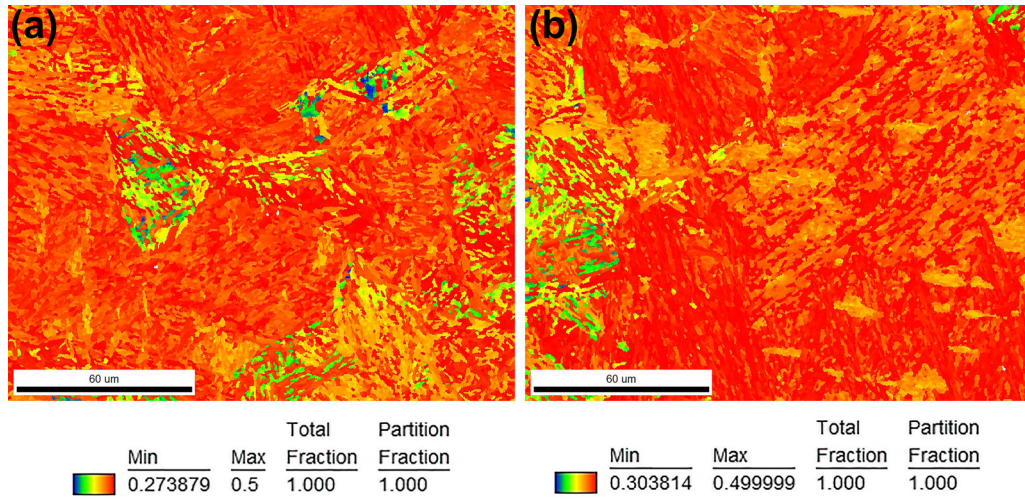


Fig. 4—SF of specimens (a) N-10 and (b) S-10 based on EBSD analysis.

Table I. M_s , Normalized Fractions of Martensite, and Amount of RA in Different Specimens

| Specimens | N-1 | N-5 | N-10 | S-1 | S-5 | S-10 |
|------------------|----------|----------|----------|----------|----------|----------|
| M_s (°C) | 261 ± 5 | 252 ± 4 | 237 ± 3 | 273 ± 7 | 260 ± 6 | 245 ± 3 |
| Martensite (Pct) | 60.8 ± 2 | 65 ± 3 | 77.6 ± 5 | 70.1 ± 3 | 77.1 ± 4 | 83.8 ± 5 |
| RA (Pct) | 22.9 ± 3 | 19.7 ± 2 | 17.6 ± 2 | 15.3 ± 2 | 9.3 ± 1 | 7.9 ± 1 |

The staying time of the specimen in the high-temperature region is longer at a low cooling rate, causing the growth of austenite grains and the reduction of dislocations and defects in grains.^[24] Moreover, carbon atoms diffuse more easily at high temperature and it is difficult to form Cottrell atmosphere. Coarse austenite grains and less Cottrell atmosphere result in the decrease of austenite strength. According to Reference 4, the M_s increases at a smaller austenite strength. Therefore, the M_s is higher at a low cooling rate. Regarding the M_s change at different cooling rates under stress, besides the preceding reasons, MT is promoted by additional mechanical driving and more nucleation sites induced by small deformation at high temperature.^[25] Therefore, the M_s increases with the decrease of cooling rate.

The mechanical driving force (ΔG_{mech}) induced by applied stress is comprised of two terms: $\tau\gamma$ is the product of the shear stress resolved along a potential habit plane by the transformation shear strain, and $\sigma\varepsilon$ is the product of the normal stress resolved perpendicular to the habit plane by the normal component of the transformation strain. Thus,

$$\Delta G_{\text{mech}} = \tau\gamma + \sigma\varepsilon \quad [2]$$

The dilation strain (ε) for MT is calculated using the following equations^[26]:

$$\Delta = \frac{\rho_A - \rho_M}{\rho_M} \quad [3]$$

$$\varepsilon = \Delta + \left[(1 + \Delta)^2 \sin^2 \gamma + \Delta^2 \right] / 2 \quad [4]$$

where Δ is the transformation volume change and ρ_A and ρ_M are the densities of the austenite and martensite phases, respectively. $\gamma(0.22)$ is obtained in Reference 27. Thus, ε is calculated to be 0.0515.

For uniaxial tension or compression, the resolved shear and normal stresses can be obtained by considering Mohr's circle:

$$\tau = \frac{1}{2} \sigma_1 \sin 2\theta \quad [5]$$

$$\sigma = \pm \frac{1}{2} \sigma_1 (1 + \cos 2\theta) \quad [6]$$

where σ_1 is the value of the applied stress (tension or compression) and θ is the angle between the specimen axis and the normal to any potential habit plane.

Therefore, ΔG_{mech} may be expressed as a function of the orientation of a transforming martensitic plate:

$$\Delta G_{\text{mech}} = \frac{1}{2} \gamma \sigma_1 \sin 2\theta + \frac{1}{2} \varepsilon \sigma_1 (1 + \cos 2\theta) \quad (\text{tension stress}) \quad [7]$$

$$\Delta G_{\text{mech}} = \frac{1}{2} \gamma \sigma_1 \sin 2\theta - \frac{1}{2} \varepsilon \sigma_1 (1 + \cos 2\theta) \quad (\text{compressive stress}) \quad [8]$$

Since we are concerned with the plates that form first (at the M_s) under the influence of applying stress, it is

necessary to find the particular orientation that yields a maximum value of ΔG_{mech} :

$$\frac{d\Delta G_{\text{mech}}}{d\theta} = \gamma\sigma_1 \cos 2\theta \pm \varepsilon\sigma_1(1 - \cos 2\theta) \quad [9]$$

$$\tan 2\theta = \frac{\sin 2\theta}{\cos 2\theta} = \pm \frac{\gamma}{\varepsilon} \quad [10]$$

The maximal mechanical driving force is obtained when $\tan 2\theta = \pm \gamma/\varepsilon$ is satisfied. Thus, the optimal θ were calculated to be 37.98 deg (for tensile stress) and 52.02 deg (for compressive stress). The maximal mechanical driving force (ΔG_{mech}) was obtained to be 60.2 J/mol for the compressive stress of 70 MPa.

According to Eq. [11], the angle of λ is calculated to be 37.98 deg because the value of θ is 52.02 deg. Thus, the orientation factor m , *i.e.*, Schmid factors (SFs), is calculated to be 0.48.

$$m = \cos \theta \cos \lambda \quad [11]$$

where m is the orientation factor and λ is the angle between the stress axis and the shear stress direction along the potential habit plane. Figure 4 gives the SF of specimens N-10 and S-10 based on EBSD analysis. The result demonstrates that the value of SF is increased by applying stress, and the SF in specimen S-10 is closer to

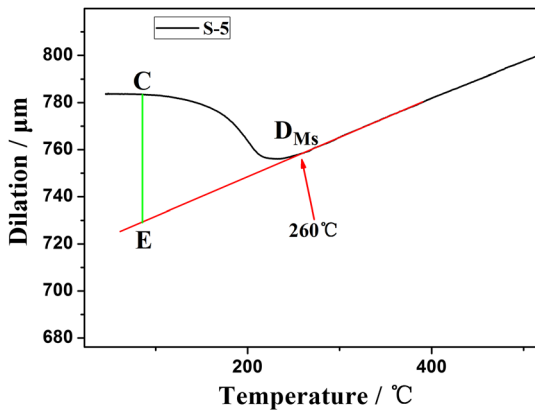


Fig. 5—Example for the normalized dilation amount of martensite.

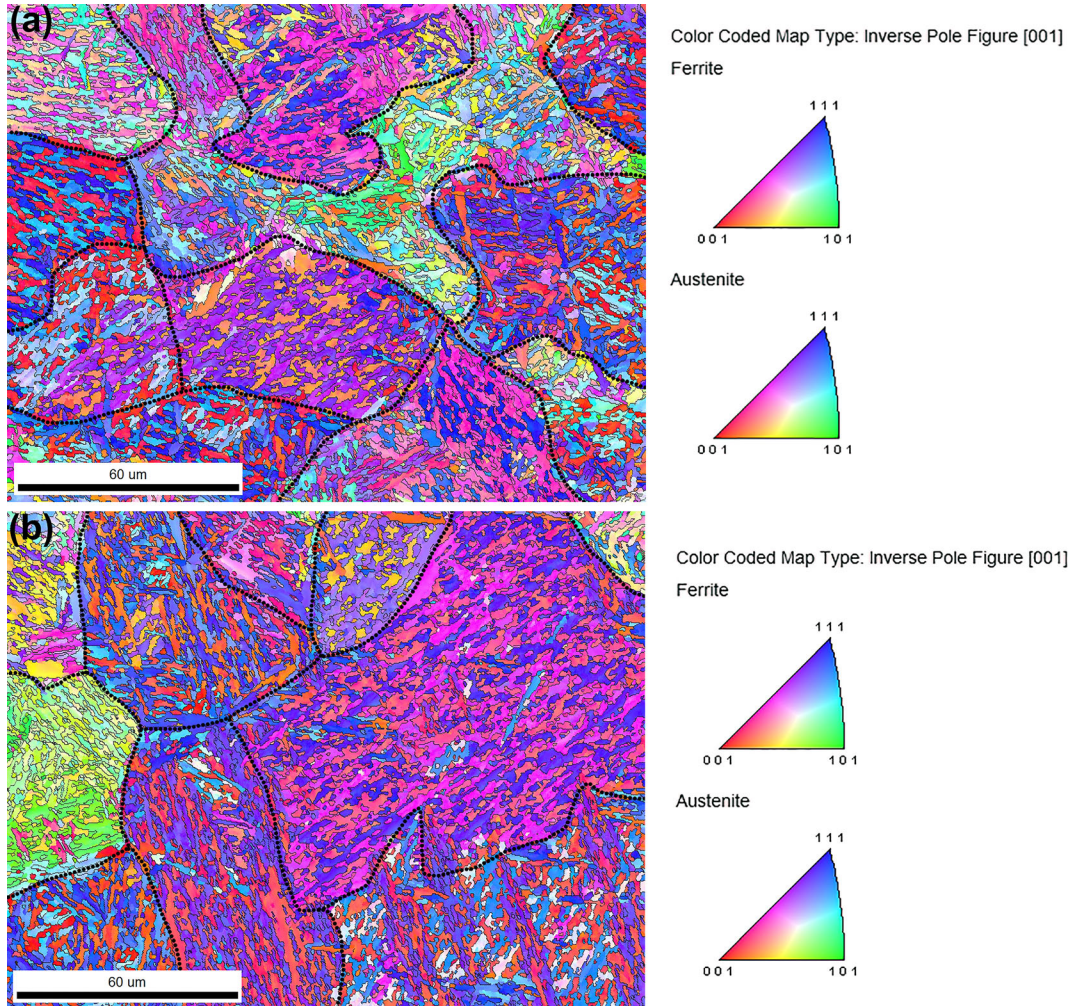


Fig. 6—Orientation map of specimens (a) N-10 and (b) S-10.

the calculated value by theoretical formulas than that in specimen N-10.

Regarding the M_s at the same cooling rate, when stress is applied on specimens during cooling, the stress provides additional mechanical driving force of 60.2 J/mol, which induces MT and causes the increase in the M_s . At the same time, it has been proved that the M_s increases after ausforming with small strain,^[25] resulting in the acceleration of MT. In this study, applying stress of 70 MPa during continuous cooling led to small plastic deformation (less than 5 pct strain) because of the low yield strength of austenite at high temperature. Hence, the MT is promoted by more nucleation sites induced by small deformation. Therefore, the M_s of specimens S-1, S-5, and S-10 increases under stress at the same cooling rate compared with specimens N-1, N-5, and N-10.

Due to the different diameter of specimens before MT, the dilation amounts in Figure 3 should be normalized in order to compare the amount of MT at different stress states and cooling rates. The dilation amount is the result of the combined effect of expansion caused by MT and contraction caused by cooling. Thus, the actual dilation amount of MT is the sum of dilation and contraction amounts. As shown in Figure 5, point C to E (D_{CE}) is the absolute dilation caused by MT. The dilation amounts were normalized by dividing D_{CE} by the diameter of the sample at the M_s , and the results are shown in Table I. The normalized dilation represents the amount of MT. It is observed that the amount of MT increases with the increase of cooling rates, while the M_s decreases. This is because a larger driving force is provided for MT due to the lower M_s at the faster

cooling rate, resulting in the formation of more martensite. On the other hand, a higher degree of supercooling makes the MT more intense and a higher latent heat is generated simultaneously, which is beneficial to the formation of more martensite.^[28] Hence, more martensite forms at the faster cooling rate.

In addition, more martensite forms by applying stress at the same cooling rate. The MT is promoted by the additional mechanical driving force and more nucleation sites with small deformation. Besides, more martensite with stress at the same cooling rate may be related to the variants selection under stress. Therefore, more martensite forms by stress at the same cooling rate. Regarding the variants selection under stress, Figure 6 gives the orientation map of specimens N-10 and S-10. Different colors represent the different orientations of grains. It is observed that the orientation distribution of specimen N-10 is more random, and it contains more martensite variants, while the variety of martensite variants decreases and the grain orientation tends to be consistent with increasing stress from 0 to 70 MPa (specimen S-10). Hence, applying stress makes the martensite orientation tend to be consistent, resulting in variant selection.^[29–31] Figure 7 shows the corresponding inverse pole figures (IPF) of specimens N-10 and S-10. It is clear that transformation texture develops in specimen S-10 and the amount of martensite variants decreases under the effect of stress, indicating the occurrence of variant selection. Moreover, the orientation of grains is enhanced by applying stress compared to that in the specimen without stress. It can be seen that the $\langle 111 \rangle // \text{ND}$ increases with imposed stress.

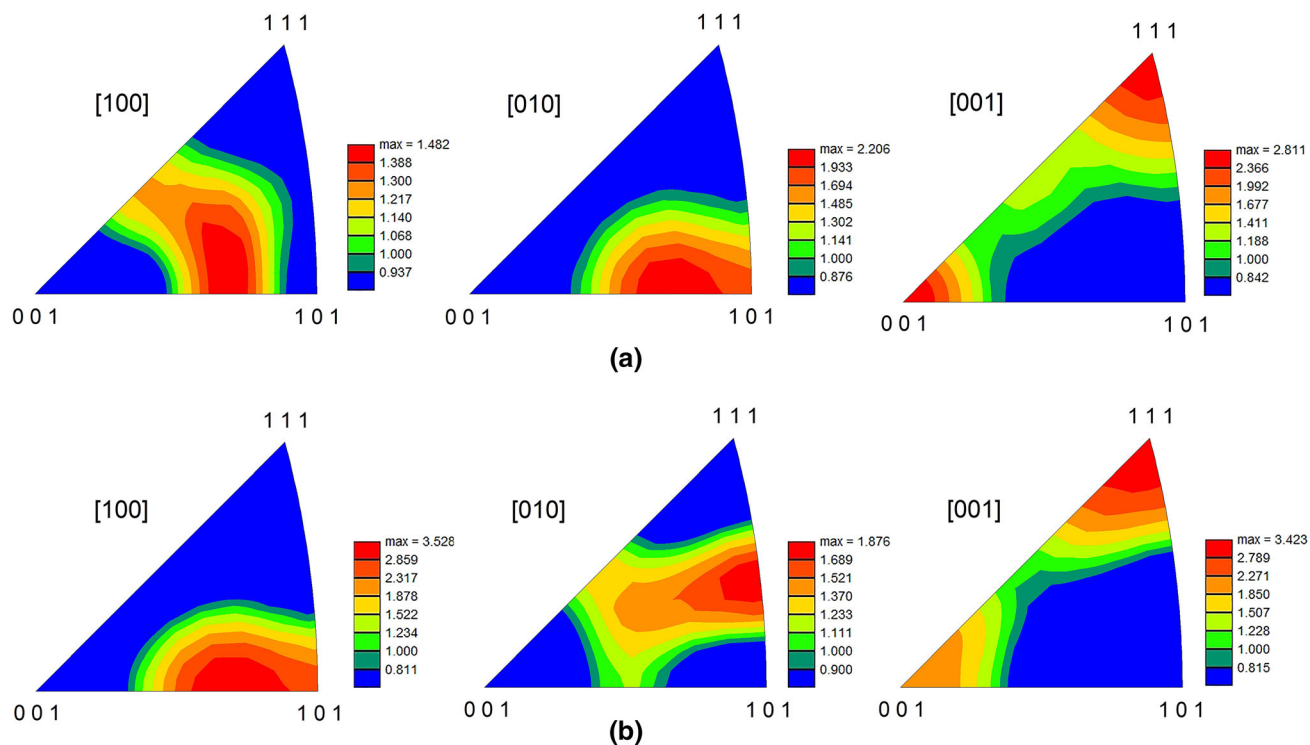


Fig. 7—IPF of specimens (a) N-10 and (b) S-10.

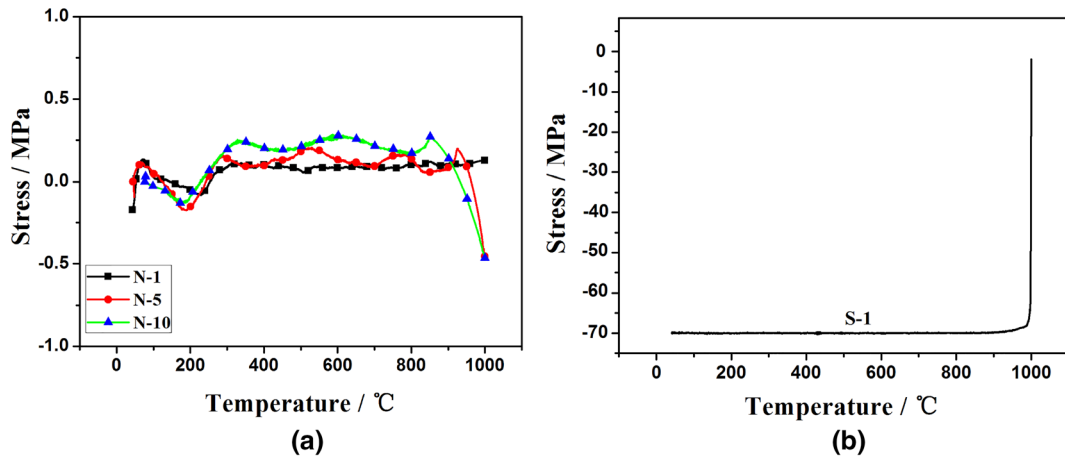


Fig. 8—(a) Stress states of specimens without stress at different cooling rates. (b) Stress state of specimen S-1 as an example.

The experiments focus on the effect of stress on MT during continuous cooling. Thus, it is necessary to analyze the stress fluctuation on specimens during the cooling process. Figure 8(a) shows the stress on specimens N-1, N-5, and N-10 during continuous cooling. It can be seen that the stress on specimens N-1, N-5, and N-10 was very small and the maximum stress was about 0.5 MPa, meaning the MT of these specimens was not affected by stress fluctuation. In addition, Figure 8(b) indicates that the magnitude of stress during continuous cooling was a constant value *vs* temperature (70 MPa). Stress loading was completed within 3 seconds for all specimens. The maximum temperature decrease was about 30 °C for S-10, indicating that the difference between the effect of the stress loading process on specimens S-1, S-5, and S-10 could be ignored.

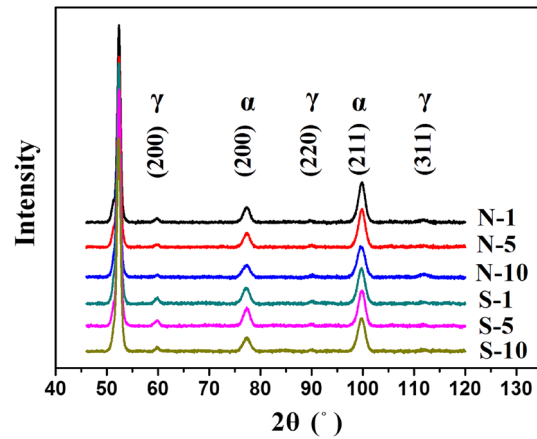


Fig. 9—Diffraction peaks of specimens.

C. XRD Experiments

Figure 9 illustrates the diffraction patterns of specimens by XRD experiments. The angles of diffraction peaks and the integrated intensities were decided using HighScore Plus software. The volume fractions of RA were calculated according to Eq. [1], and the average values of RA were obtained as the final results and are given in Table I. This shows that the volume fraction of RA decreases with the increase of cooling rate regardless of whether stress is applied. In addition, at the same cooling rate, the amount of RA in specimens with stress decreases compared to that in specimens without stress. This is because the microstructure consists of martensite and RA for all specimens; thus, more martensite means less RA at ambient temperature in specimens with stress, which is consistent with the results in dilation.

D. Mechanical Properties

Figure 10 presents the engineering stress–strain curves of different specimens. The high tensile strength is attributed to martensite transformation strengthening, fine-grain strengthening, and dislocation strengthening.^[32–34] The tensile results indicate that the tensile strength at the same cooling rate is improved

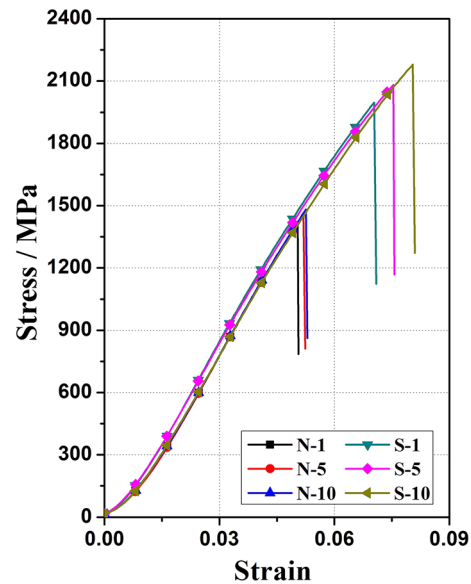


Fig. 10—Engineering stress–strain curves of different specimens.

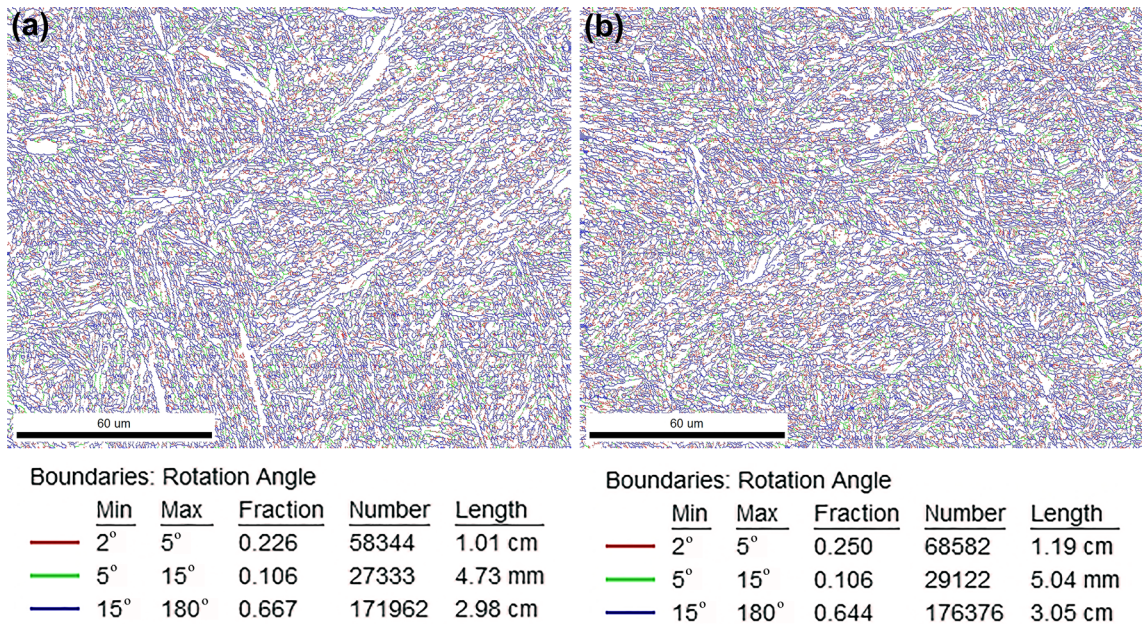


Fig. 11—Distribution of grain boundaries of different specimens: (a) N-10 and (b) S-10.

significantly by stress compared to that of specimens without stress. This is because the martensite amount of specimens with stress is larger than that of specimens without stress and martensite laths are finer in specimens with stress, resulting in higher strength in specimens with stress. In addition, reasons for brittle fracture characteristics of specimens during tensile tests are as follows. The microstructure consists of two phases: hard martensite and soft RA. RA is induced to be martensite by stress and RA is gradually consumed before yielding during the tensile test.^[35,36] Thus, the microstructure is basically composed of martensite before yielding, resulting in the occurrence of brittle fracture characteristics. Besides, Figure 11 gives the distribution of grain boundaries of different specimens. It shows that the fraction of low-angle grain boundaries increases by stress, which is also beneficial to the strength.^[37] Moreover, the strength improvement (from about 1990 to 2170 MPa) with the increase of cooling rate was relatively larger under stress compared with specimens without stress. This may be attributed to more dislocations and defects in specimen S-10 due to less recovery at a high cooling rate.

Figure 12 presents the fracture morphology of different specimens. It demonstrates that all specimens show the brittle fracture characterization. Although RA exists in microstructure, martensite forms during the quenching process and no subsequent tempering process is followed, resulting in higher dislocation density inside the martensite grain. Thus, all specimens exhibit brittle

fracture characterization. It is seen that an obvious cleavage fracture occurs in specimens without stress. In addition, the size of the cleavage plane is larger in stress-free specimens compared to that in specimens with stress. Moreover, a decrease of the cleavage plane is observed with increasing cooling rates under stress state. Fracture morphology is consistent with the results of the tensile test.

IV. CONCLUSIONS

The effects of applying external stress on martensite transformation and the mechanical response of a medium-carbon high-strength steel during continuous cooling were investigated by metallography, dilatometry, XRD, and tensile tests. The following conclusions were obtained.

1. The M_s was increased by stress due to additional mechanical driving force. The martensite transformation was promoted and the martensite amount increased by applying stress, while the amount of RA decreased at the same cooling rate.
2. The martensite laths were refined and martensite orientation tended to be consistent due to variant selection by applying stress.
3. The tensile strength increased from about 1470 to 2170 MPa by applying stress because of more martensite and a greater fraction of low-angle grain boundaries.

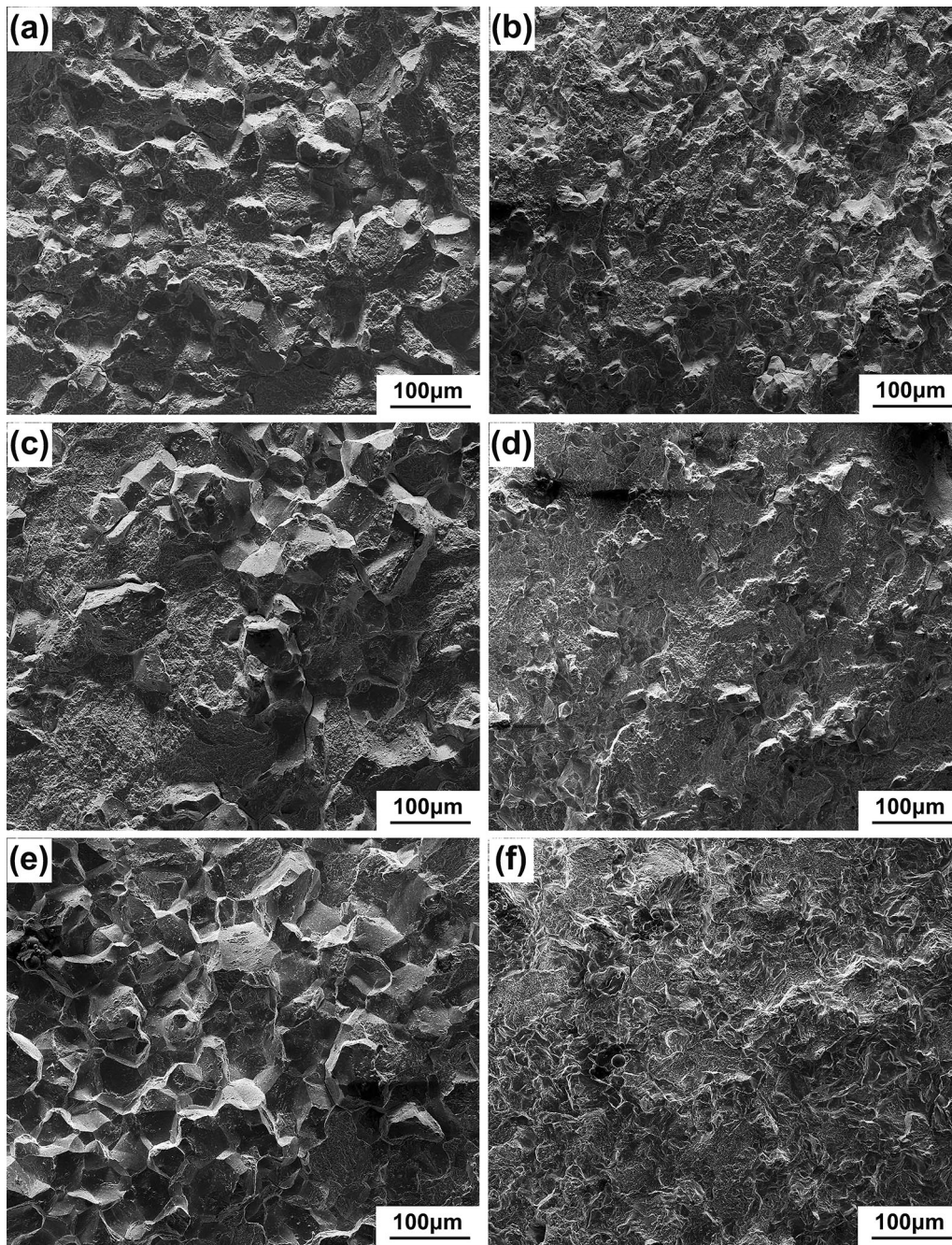


Fig. 12—Tensile fractures of different specimens: (a) N-1, (b) S-1, (c) N-5, (d) S-5, (e) N-10, and (f) S-10.

ACKNOWLEDGMENTS

The authors gratefully acknowledge the financial support from the National Natural Science Foundation of China (NSFC) (Grant Nos. 51874216 and 51704217), the Major Projects of Technology Innovation of Hubei Province (Grant No. 2017AAA116), and the Hebei Joint Research Fund for Iron and Steel (Grant No. E2018318013).

REFERENCES

1. F. Maresca, V.G. Kouznetsova, M.G.D. Geers, and W.A. Curtin: *Acta Mater.*, 2018, vol. 156, pp. 463–78.
2. S. Sharma, B.R. Kumar, B.P. Kashyap, and N. Prabhu: *Mater. Sci. Eng. A*, 2018, vol. 725, pp. 215–27.
3. J.Y. Tian, G. Xu, Z.Y. Jiang, H.J. Hu, Q. Yuan, and X.L. Wan: *Metall. Mater. Int.*, 2019, <https://doi.org/10.1007/s12540-019-00370-8>.
4. H.S. Yang and H.K.D.H. Bhadeshia: *Scripta Mater.*, 2009, vol. 60, pp. 493–95.

5. X. Li, L. Chen, Y. Zhao, X. Yuan, and M.R.D. Kumar: *Mater. Sci. Eng. A*, 2018, vol. 715, pp. 257–65.
6. J. Huang and Z. Xu: *Mater. Sci. Eng. A*, 2006, vol. 438, pp. 254–57.
7. G.S. Ansell, P.J. Brofman, T.J. Nichol, and G. Judd: *Int. Conf. on Martensitic Transformations ICOMAT '79*, G.B. Olson and M. Cohen, eds., 1979, pp. 350–55.
8. M. Nikraves, M. Naderi, and G.H. Akbari: *Mater. Sci. Eng. A*, 2012, vol. 540, pp. 24–29.
9. K.W. Andrews: *Iron Steel Inst.*, 1965, vol. 203, pp. 721–27.
10. C. Capdevila, F.G. Caballero, and C. Garcia De Andrés: *Mater. Sci. Technol.*, 2003, vol. 19, pp. 581–86.
11. D.J.C. Mackay: *Neural Comput.*, 2014, vol. 4, pp. 448–72.
12. G. Ghosh and G.B. Olson: *Acta Mater.*, 2002, vol. 50, pp. 2655–75.
13. J. Wang, P.J.V.D. Wolk, and S.V.D. Zwaag: *J. Mater. Sci.*, 2000, vol. 35, pp. 4393–4404.
14. G.B. Olson and M. Cohen: *Metall. Trans. A*, 1976, vol. 7A, pp. 1897–1904.
15. S. Chatterjee, H.S. Wang, J.R. Yang, and H.K.D.H. Bhadeshia: *Mater. Sci. Technol.*, 2006, vol. 22, pp. 641–44.
16. M. Zhang, Y.H. Wang, C.L. Zheng, F.C. Zhang, and T.S. Wang: *Mater. Sci. Eng. A*, 2014, vol. 596, pp. 9–14.
17. M. Maalekian, E. Kozeschnik, S. Chatterjee, and H.K.D.H. Bhadeshia: *J. Met. Sci.*, 2007, vol. 23, pp. 610–12.
18. C. Zhang, D. Cai, Y. Wang, M. Liu, B. Liao, and Y. Fan: *Mater. Charact.*, 2008, vol. 59, pp. 1638–42.
19. S.H.M. Anijdan, A. Rezaeian, and S. Yue: *Mater Charact.*, 2012, vol. 63, pp. 27–38.
20. S. Masoud and D.S. Mersagh: *J. Manuf. Process.*, 2018, vol. 34, pp. 313–28.
21. M. Wang, G. Xu, L. Wang, Y.W. Xu, and Z.L. Xue: *J Wuhan Univ Technol*, 2017, vol. 32, pp. 186–89.
22. C.Y. Wang, J. Shi, W.Q. Cao, and H. Dong: *Mater. Sci. Eng. A*, 2010, vol. 527, pp. 3442–49.
23. F.R. Xiao, L. Bo, Y.Y. Shan, and K. Yang: *Mater Charact.*, 2005, vol. 54, pp. 417–22.
24. Y. Yan, G.L. Jiang, T.F. Guo, L.L. Zhang, and S.K. Wei: *Heat Treat. Met.*, 2018, vol. 43, pp. 199–204 (in Chinese).
25. B.B. He, W. Xu, and M.X. Huang: *Mater. Sci. Eng. A*, 2014, vol. 609, pp. 141–46.
26. F. Marketz and F.D. Fischer: *Metall. Mater. Trans. A*, 1995, vol. 26A, pp. 267–78.
27. E.S. Machlin and M. Cohen: *JOM*, 1951, vol. 3, pp. 746–54.
28. S.J. Lee and Y.K. Lee: *Scripta Mater.*, 2009, vol. 60, pp. 1016–19.
29. S. Kundu, A.K. Verma, and V. Sharma: *Metall. Mater. Trans. A*, 2012, vol. 43A, pp. 2552–65.
30. S. Kundu and H.K.D.H. Bhadeshia: *Scripta Mater.*, 2007, vol. 57, pp. 869–72.
31. G. Miyamoto, N. Iwata, N. Takayama, and T. Furuhashi: *J. Alloys Comps.*, 2013, vol. 577, pp. 528–32.
32. Z.Y. Tang, J.N. Huang, H. Ding, Z.H. Cai, and R.D.K. Misra: *Mater. Sci. Eng. A*, 2018, vol. 724, pp. 95–102.
33. L. Qi, A.G. Khachaturyan, and J.W. Morris: *Acta Mater.*, 2014, vol. 76, pp. 23–39.
34. B.B. He and M.X. Huang: *Metall. Mater. Trans. A*, 2015, vol. 46A, pp. 688–94.
35. M. Sabzil and M. Farzam: *Mater Res Expr*, 2019, vol. 6, pp. 1–15.
36. S.H.M. Anijdan and S. Yue: *Metall. Mater. Trans. A*, 2012, vol. 43A, pp. 1140–62.
37. S.C. Li, C.Y. Guo, L.L. Hao, Y.L. Kang, and Y.G. An: *Mater. Sci. Eng. A*, 2019, vol. 759, pp. 624–32.

Publisher's Note Springer Nature remains neutral with regard to jurisdictional claims in published maps and institutional affiliations.